

Article

An Experimental and a Kinetic Modelling Study of Ethanol/Acetone/Ethyl Acetate Mixtures

Yangxun Liu ¹, Weinan Liu ², Huihong Liao ³, Hasier Ashan ², Wenhua Zhou ² and Cangsu Xu ^{2,*}¹ Zhejiang Technical Institute of Economics, Hangzhou 310018, China; 240064@zjtie.edu.cn² College of Energy Engineering, Zhejiang University, Hangzhou 310027, China; 21927051@zju.edu.cn (W.L.); 3180106002@zju.edu.cn (H.A.); zwh114@zju.edu.cn (W.Z.)³ Vehicle Engineering Center-CAE Technology Development, Geely Automobile Research Institute, Ningbo 315336, China; colinliao027@163.com

* Correspondence: xucangsu@zju.edu.cn

Abstract: With the world's energy resources decreasing, ethanol/acetone/ethyl acetate mixed fuel has the potential as a fossil fuel alternative or oxygenated fuel additive. In this work, the burning characteristics of ethanol/acetone/ethyl acetate mixed fuels including 3 pure fuels, 9 binary fuels, and 7 ternary fuels were studied at a temperature of 358 K, the pressure of 1 bar, and the equivalence ratios of 0.7 to 1.4 in the constant volume combustion chamber (CVCC). The burning velocities of the ternary fuels were compared at $\phi = 0.8, 1.0, \text{ and } 1.4$. The results show that the laminar burning velocities of the mixed fuels are affected by the contents of ethanol, acetone, and ethyl acetate. The Markstein length, Markstein number, and burning flux were also analyzed in this paper. Furthermore, a detailed chemical mechanism comprising 506 species and 2809 reactions was reduced to a skeletal mechanism including 98 species and 642 reactions, using the directed relation graph with error propagation (DRGEP). The experimental and the simulated laminar burning velocities were compared. The results of laminar burning velocities show that the relative deviation of ETEAAC 112 is approximately 17.5%. The sensitivity coefficients, flame structure, and reaction paths of ethyl acetate were investigated with the skeletal and the detailed mechanisms. It is found that the key reaction path is retained in the skeletal mechanism.

Keywords: ethanol; acetone; ethyl acetate; mechanism reduction; laminar burning velocity



Citation: Liu, Y.; Liu, W.; Liao, H.; Ashan, H.; Zhou, W.; Xu, C. An Experimental and a Kinetic Modelling Study of Ethanol/Acetone/Ethyl Acetate Mixtures. *Energies* **2022**, *15*, 2992. <https://doi.org/10.3390/en15092992>

Academic Editors: Amin Paykani and Rob J.M. Bastiaans

Received: 16 February 2022

Accepted: 15 April 2022

Published: 20 April 2022

Publisher's Note: MDPI stays neutral with regard to jurisdictional claims in published maps and institutional affiliations.



Copyright: © 2022 by the authors. Licensee MDPI, Basel, Switzerland. This article is an open access article distributed under the terms and conditions of the Creative Commons Attribution (CC BY) license (<https://creativecommons.org/licenses/by/4.0/>).

1. Introduction

Fossil fuels such as oil, natural gas, coal, etc., are the main energy sources. However, the extensive, long-term use of fossil fuels has caused significant environmental pollution and other related problems [1,2], which has increased the research to find alternative fuels. Therefore, researchers have turned their attention to alternative green fuels like ethanol/acetone/ethyl acetate mixture, which is the intermediate product from the synthesis of biomass pyrolysis oil [3,4].

Ethanol, acetone, and ethyl acetate might be alternative fuels in the future. As an alternative to gasoline, ethanol has a higher octane number than gasoline [5,6]. Ethanol-gasoline blended fuel can increase the compression ratio to achieve a higher combustion efficiency and to increase engine output torque [7,8]. An ethanol-gasoline fuel mixture can reduce HC, CO, and NO_x emissions [9,10]. Moreover, an acetone and a gasoline fuel mixture can significantly improve engine performance. Although HC and CO emissions are higher at idle speed, as the engine speed increases, its emissions are significantly lower compared to pure gasoline [11–13].

The combustion characteristics of ethanol have been investigated by many researchers. Sekularac et al. [14] used Le Châtelier mixing empirical correlation to calculate the laminar burning velocity (LBV) of ethanol mixtures (iso-octane/ethanol). They found that the LBV predicted by the mixing law agreed well with the experimental results. Katoch et al. [15]

measured the LBV of ethanol at high temperatures using the diverging channel method, and the results showed that the temperature exponents exhibited a parabolic trend with the minimum value at the equivalence ratio of 1.1. Aghsaei et al. [16] examined the LBV of ethanol at the pressure of 1, 2, and 5 bar and an initial temperature of 318–473 K. It was found that increased temperature increased the unstretched flame speed. Knorsch et al. [17] investigated the combustion mechanisms and the burning behavior of ethanol. The study showed that the LBV decreased linearly up to 50% at a 20% EGR (exhaust gas recirculation) rate. Sileghem et al. [18] reported the LBV of ethanol and its binary/quaternary mixtures (ethanol–hydrocarbon blends), and they found that the energy fraction mixing rules predicted the experimental data accurately. Dirrenberger et al. [19] used the heat flux method to measure the LBV of gasoline/ethanol mixtures and indicated that ethanol addition showed a negligible effect on gasoline.

Regarding acetone, Zhang et al. [20] studied the premixed flame characteristics of acetone mixtures. The results showed that with an increased concentration of acetone in acetone–butanol–ethanol mixtures, the diffusional thermal stability reduced. Nilsson et al. [21] investigated the LBV of acetone at a pressure of 1 atm, the temperature of 298, 318, 338, and 358 K. Nilsson et al. [21] found that H-abstraction reactions forming acetyl radicals and $\text{CH}_3\text{COCH}_3 = \text{CH}_2\text{CO} + \text{CH}_4$ were the two significant reactions for decomposition. Zhang et al. [22] compared the LBV of acetone, n-butanol, and ethanol, and they indicated that the LBVs of the three fuels followed the order of ethanol > n-butanol > acetone. Moreover, Gong et al. [23] analyzed the combustion characteristics of acetone. The study revealed that the formation of methyl radical was the main reason for lower LBVs of acetone compared with that of n-propanol and propanal.

Ethyl acetate has been investigated in some studies. Ahmed et al. [24] investigated the combustion of ethyl acetate at a temperature of 1200 K and a pressure of 15 bar. The authors found that unimolecular decomposition was the dominant reaction pathway that consumed ethyl acetate to form ethylene and acetic acid. Wang et al. [25] studied the oxidation characteristics of ethyl acetate using kinetic models and the counterflow configuration. It was found that large amounts of CH_3 were produced from ethyl acetate oxidation. Osipova et al. [26] measured the combustion intermediates of ethyl acetate, reporting that the decomposition of the fuel radicals was the same under near-stoichiometric and fuel-rich conditions. Xu et al. [27] reported the combustion characteristics of ethyl acetate using outward propagating spherical flames, and they found that hydrodynamic instability was intense at $\phi = 1.1$.

To investigate premixed flame characteristics of ethanol/acetone/ethyl acetate mixture as a potential fuel or oxygenated fuel additive, studies on its combustion performance have been performed. To the best knowledge of the authors, this is the first paper to study the laminar burning characteristics of ternary mixed fuels (ethanol/acetone/ethyl acetate) and to conduct an in-depth analysis of the detailed/skeletal chemical reaction mechanism. The constant volume combustion chamber combined with the high-speed schlieren imaging system is used to measure the laminar premixed characteristics of the refined biomass pyrolysis oil (ethanol, ethyl acetate, and acetone). The main laminar premixed characteristics investigated include laminar burning velocity, Markstein length, Markstein number, burning flux, etc., at $T_0 = 358$ K and $P_0 = 1$ atm. The skeletal mechanism is obtained by the directed relation graph with error propagation (DRGEP) using Chemkin software. The chemical reaction paths of the skeletal mechanism and the detailed mechanism are compared and analyzed.

2. Experimental Set-Up

The experimental device used in this study is shown in Figure 1. The setup had a constant volume combustion chamber with an internal volume of 1.94 L and a high-speed camera in a schlieren imaging system for recording the flame images. The side of the constant volume combustion chamber was equipped with a quartz window for optical access. Heating rods with a rated power of 60 W were uniformly arranged on each side of

the constant volume combustion chamber. A K-type thermocouple and a pressure sensor were installed outside the constant volume combustion chamber. The temperature in the combustion chamber was monitored with the K-type thermocouple and a temperature display. The pressure sensor (Kistler 6115A) worked with a charge amplifier to record the pressure data of the combustion process and to display it on the oscilloscope. During the experiment, the triggering of the ignition signal was controlled by the computer and the digital delay generator. An ignition electrode wire (platinum wire) was installed in the center of the constant volume combustion chamber, and the ignition energy was set to approximately 15 mJ. When the combustion process was complete, the exhaust gas was discharged through the exhaust system. More information on the experimental system can be found in Refs. [28–30]. According to the components of the mixed fuels, 18 fuel groups are selected in this study, including 3 pure fuels, 9 binary fuels, and 7 ternary fuels (see Table 1).

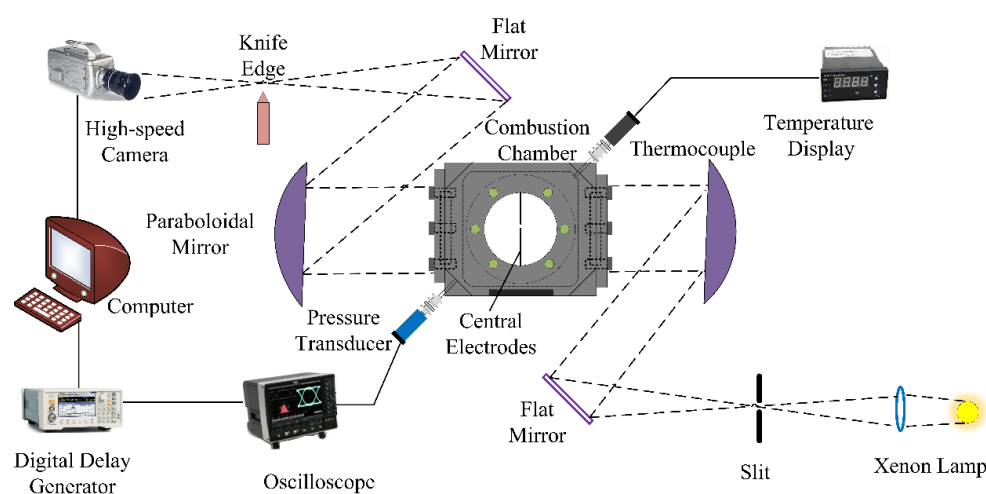


Figure 1. The system of the experimental set-up.

Table 1. Fuels with different components tested in this study.

Fuel Group	Ethanol (ET)/Vol.	Acetone (AC)/Vol.	Ethyl Acetate (EA)/Vol.
ET	100%	-	-
AC	-	100%	-
EA	-	-	100%
ETAC13	25%	75%	-
ETAC11	50%	50%	-
ETAC31	75%	25%	-
ETEA13	25%	-	75%
ETEA11	50%	-	50%
ETEA31	75%	-	25%
ACEA13	-	25%	75%
ACEA11	-	50%	50%
ACEA31	-	75%	25%
ETEAAC211	50%	25%	25%
ETEAAC121	25%	25%	50%
ETEAAC112	25%	50%	25%
ETEAAC221	40%	20%	40%
ETEAAC212	40%	40%	20%
ETEAAC122	20%	40%	40%
ETEAAC111	33.33%	33.33%	33.34%

3. Data Processing

The flame front recorded with the schlieren imaging was detected using Matlab software and the pixels surrounded by the spherical flame could be measured. The radius of the spherical flame R_f can be calculated as:

$$R_f = \sqrt{\frac{A_f}{A_a}} R_0 \quad (1)$$

where A_f is the pixels surrounded by flame front, R_0 is the radius of the quartz window, A_a is the total pixel points contained in the window; R_0 is 45 mm in this study. The stretched flame burning velocity (S_b) is obtained with Equation (2),

$$S_b = \frac{dR_f}{dt} \quad (2)$$

where t is the flame propagation time. The flame stretch rate (κ) is calculated as [31]:

$$\kappa = 2 \frac{S_b}{R_f} \quad (3)$$

Using the linear extrapolation gives a slightly higher unstretched flame speed. In the current work, the non-linear extrapolation method was used to calculate the unstretched flame speed. The relationship between unstretched burning velocity S_b^0 and stretched burning velocity S_b is given in Equation (4) [32],

$$\left(\frac{S_b}{S_b^0}\right)^2 \ln\left(\frac{S_b}{S_b^0}\right) = -\frac{L_b}{S_b^0} \quad (4)$$

where L_b is the Markstein length. According to the mass conservation equation, the laminar burning velocity (u_L) is calculated using Equation (5) [33],

$$\rho_u u_L = \rho_b S_b^0 \quad (5)$$

The flame thickness (δ) is calculated with Equation (6),

$$\delta = \frac{\nu}{u_L} \quad (6)$$

where ρ_b and ρ_u are the densities of the burned and the unburned gases, respectively, and ν is the dynamic viscosity. These parameters were computed with the Chemkin software.

4. Results and Discussion

4.1. Flame Topography

Figure 2 compares the flame propagation for different ethanol concentrations at $T_0 = 358$ K, $P_0 = 1$ bar, and $\phi = 1.1$. The flame propagation speed of ETEAAC211 is the fastest, while the flame propagation speed of ETEAAC111 is the slowest, and the flame radius of ETEAAC111 is smaller at $t = 13$ ms compared with the other two fuels. Many factors affect the speed of flame propagation. Liu et al. [34] reported that the increased content of ethanol enhances the propagation speed of binary fuels. In this study, the effect of increasing ethanol content for propagation speed is not obvious for the ternary fuels. The burning velocity of the ternary fuels is affected by ethanol, acetone, and ethyl acetate, all the components play a decisive role in the laminar burning velocity of the mixed fuel. When two of these fuels have a positive effect on the burning velocity, the effect of increasing ethanol volume on the burning velocity is attenuated.

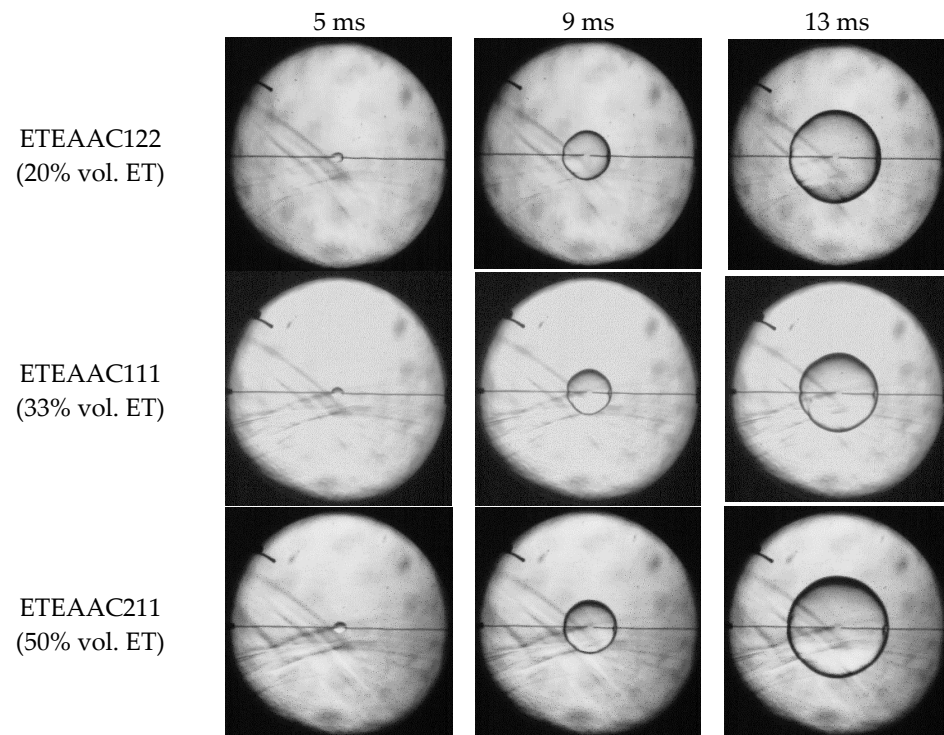


Figure 2. Flame propagation images of ETEAAC122, ETEAAC111, and ETEAAC211 at $T_0 = 358$ K, $P_0 = 1$ bar, and $\phi = 1.1$.

Figure 3 shows the flame propagation images of ETEAAC111 at $\phi = 0.7$, 1.1, and 1.4. The flame propagation speed reaches the peak at the equivalence ratio of 1.1, and the propagation speed of the rich mixture is faster than that of the lean mixture. Slight cracks appear on the flame surface at $\phi = 1.1$ and 1.4, while the flame surface is smooth at $\phi = 0.7$.

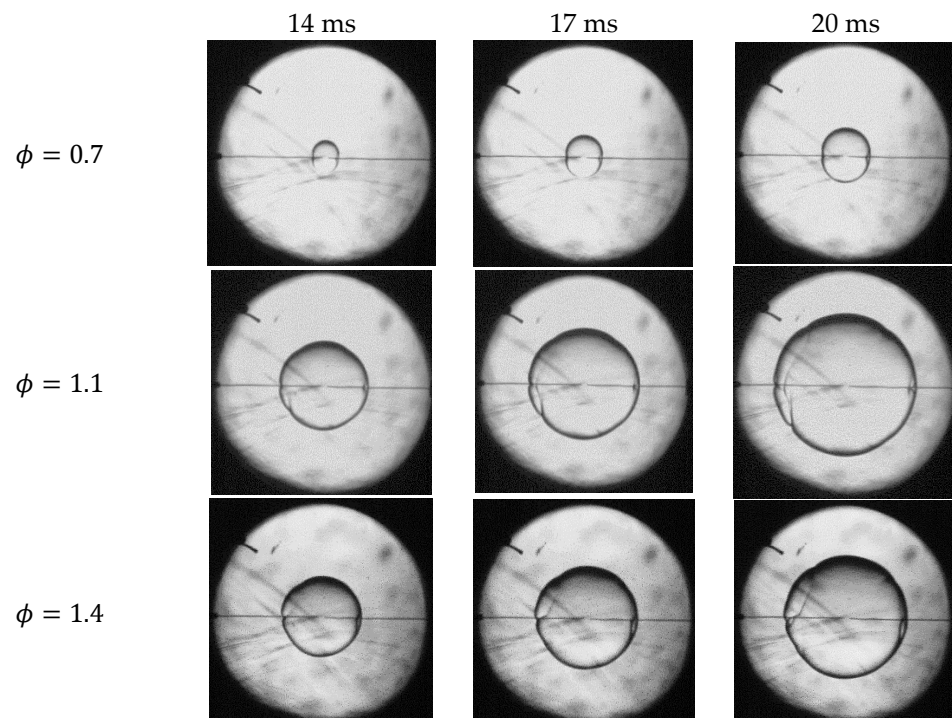


Figure 3. Flame propagation images of ETEAAC111 at $T_0 = 358$ K, $P_0 = 1$ bar, and $\phi = 0.7$, 1.1 and 1.4.

4.2. Combustion Characteristics

Figure 4 shows the ternary contour phase diagram of the laminar burning velocity at $T_0 = 358$ K, $P_0 = 1$ bar, and $\phi = 0.8, 1.0,$ and 1.4 . It can be seen from the figure that the increasing ethanol concentration increases the laminar burning velocity of the mixed fuels. However, the components of acetone and ethyl acetate reduce the laminar burning velocity of the ternary fuel. In the lean mixture, when the ethanol concentration is greater than 50%, the higher the ethyl acetate concentration, the higher the laminar burning velocity. When the ethanol concentration is less than 50%, the velocity reaches the maximum value when the ethyl acetate and acetone concentrations are close to each other, and the weakening effect of the ethyl acetate concentration on the laminar burning velocity is more obvious. In the stoichiometric mixture, the influence of ET, AC, and EA on the mixed fuel is more intuitive, and the order of the promoting effect of the concentrations of the three fuels on the laminar burning velocity is $ET > AC > EA$. In the rich mixtures, the maximum laminar burning velocity appears in the middle area of the phase diagram of the ternary contour, and the imbalance of the three fuel concentrations causes the laminar burning velocity of the ternary fuel to decrease. Overall, as the ethanol concentration increases, the laminar burning velocity slightly increases. The reason is that the C-O bond of ethanol is easier to break to form the active group OH. The concentration of OH is one of the key factors affecting the laminar burning velocity. The increase in the concentration of ethanol significantly increases the concentration of OH.

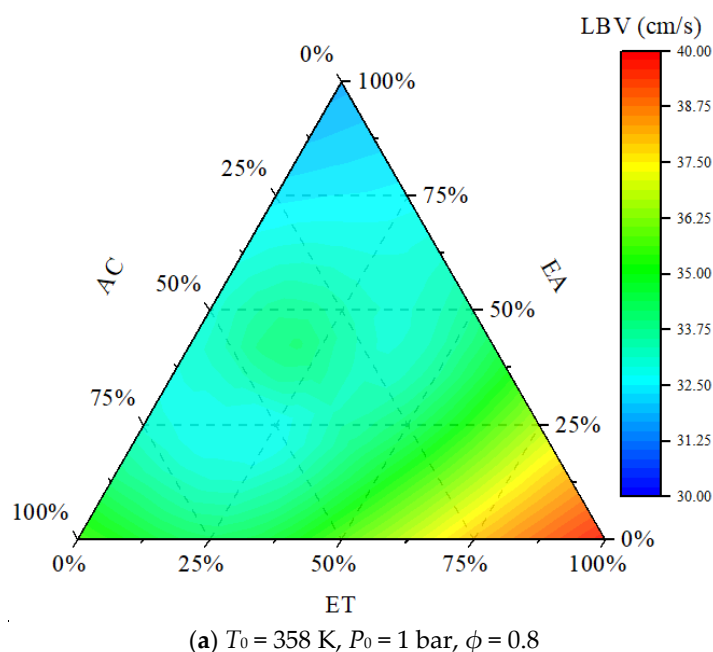


Figure 4. Cont.

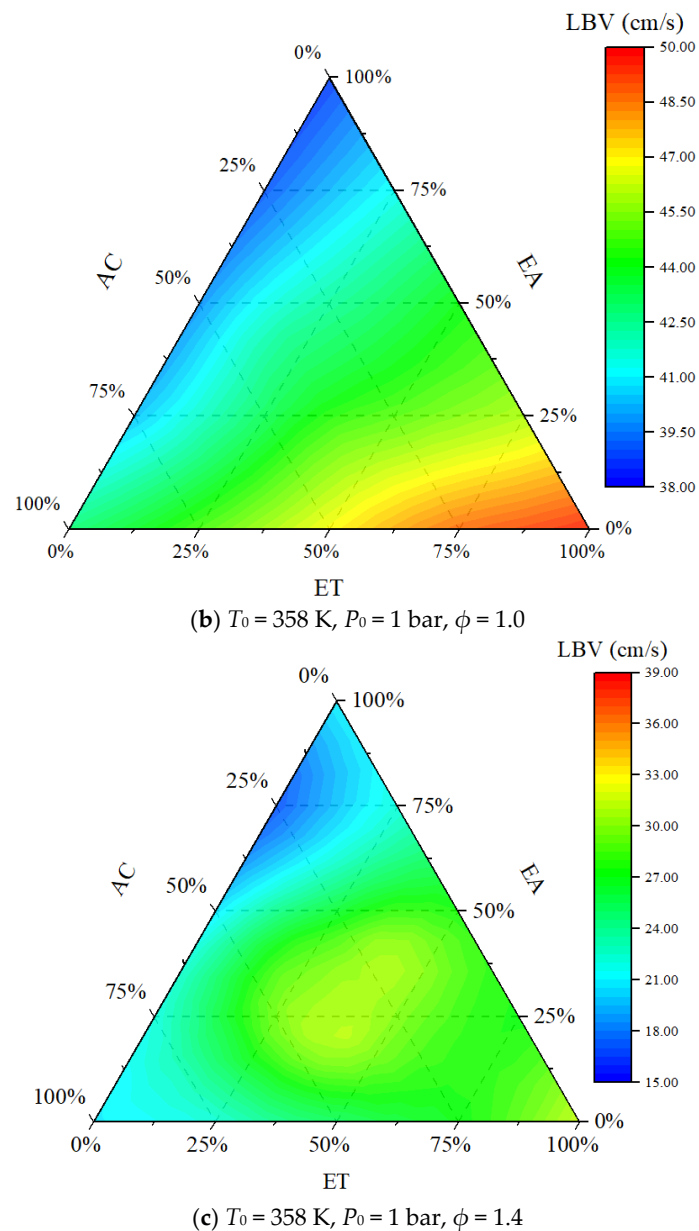


Figure 4. Ternary contour phase diagram of the laminar burning velocity at $T_0 = 358 \text{ K}$, $P_0 = 1 \text{ bar}$, and $\phi = 0.8, 1.0$, and 1.4 .

Figure 5 displays the Markstein length (L_b) and the Markstein number (M_a) of the mixed fuels at $T_0 = 358 \text{ K}$, $P_0 = 1 \text{ bar}$, and $\phi = 0.7\text{--}1.4$. The absolute value of the Markstein length characterizes the sensitivity of the flame propagation velocity to the flame stretch rate. A positive value indicates that the flame propagation velocity decreases with increasing flame stretch rate. The Markstein number ($M_a = L_b/\delta$) is determined as the ratio of the Markstein length (L_b) to the flame thickness (δ). The relationship between the Markstein length/number and the equivalence ratio is shown in Figure 5. On the lean side, the Markstein lengths are relatively close, while the Markstein lengths are significantly different on the rich side, especially when the equivalence ratio is 1.4 . Likewise, the Markstein number differs greatly on the rich side. The reason for this phenomenon is that instability of the flame occurs on the rich side of the fuel mixture. Flame instability is more obvious on the flame surface when the fuel is rich, especially for $\phi = 1.3$ and 1.4 , and the perturbation of the flame surface is more pronounced compared with lean mixtures.

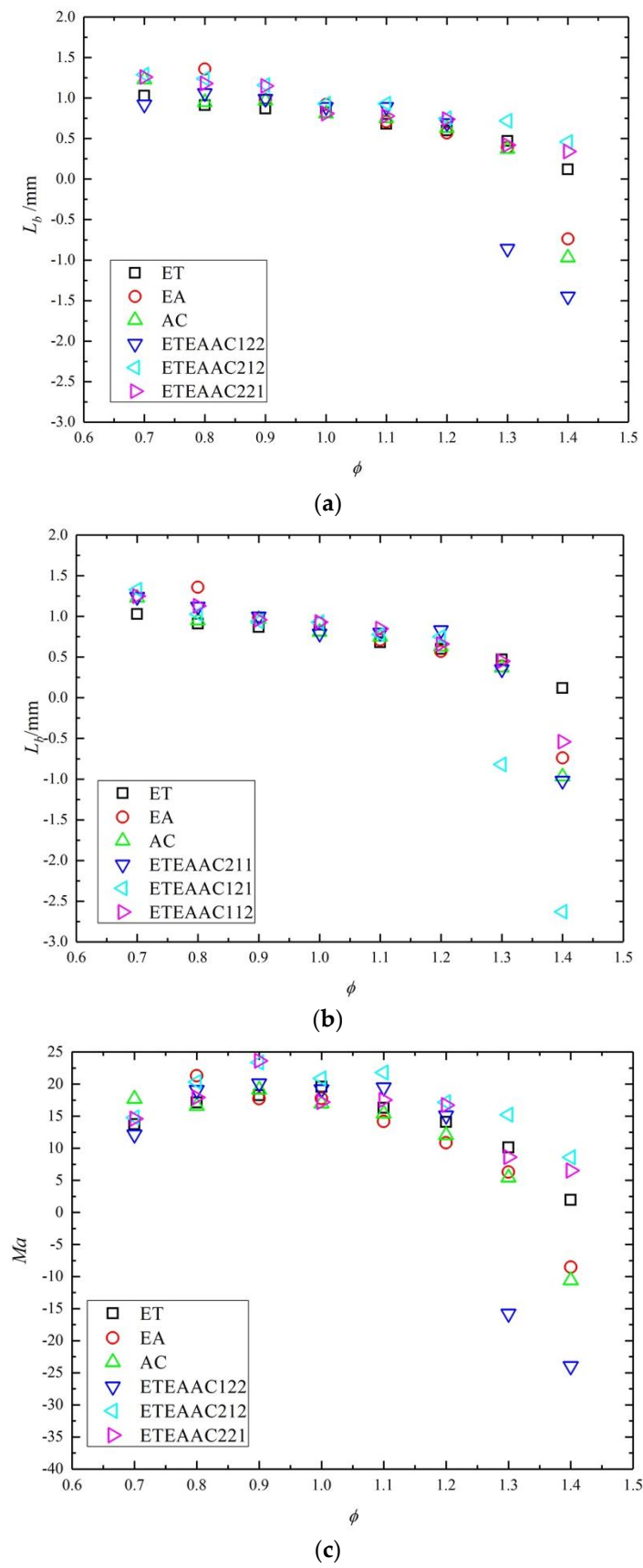


Figure 5. Cont.

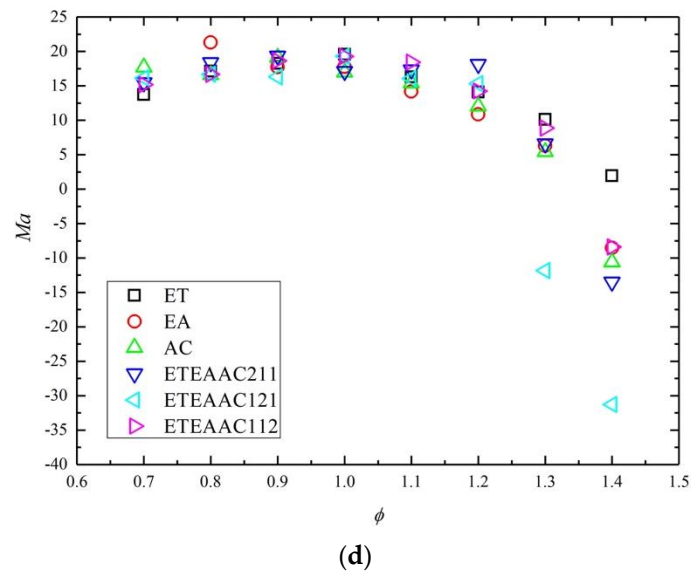


Figure 5. Markstein length and Markstein number of the ternary fuels at $T_0 = 358$ K, $P_0 = 1$ bar, and $\phi = 0.7$ – 1.4 . (a) The Markstein length of ET/EA/AC/ETEAAC122/ETEAAC212/ETEAAC221, (b) The Markstein length of ET/EA/AC/ETEAAC211/ETEAAC121/ETEAAC112, (c) The Markstein number of ET/EA/AC/ETEAAC122/ETEAAC212/ETEAAC221, (d) The Markstein number of ET/EA/AC/ETEAAC211/ETEAAC121/ETEAAC112.

Figure 6 shows the laminar burning flux of the ternary fuels with the equivalence ratios. The laminar burning flux ($f = u_L \rho_u$) is calculated as the product of the laminar burning velocity and the density of the unburned mixture. Since the density of the unburned mixture of the fuels reported in this paper is not much different, the trend of the laminar burning flux is consistent with that of the laminar burning velocity. The maximum laminar burning flux appears at the equivalence ratio of 1.0–1.2, and the laminar burning flux of ETEAAC mixed fuel is closer to the pure fuels on the lean side.

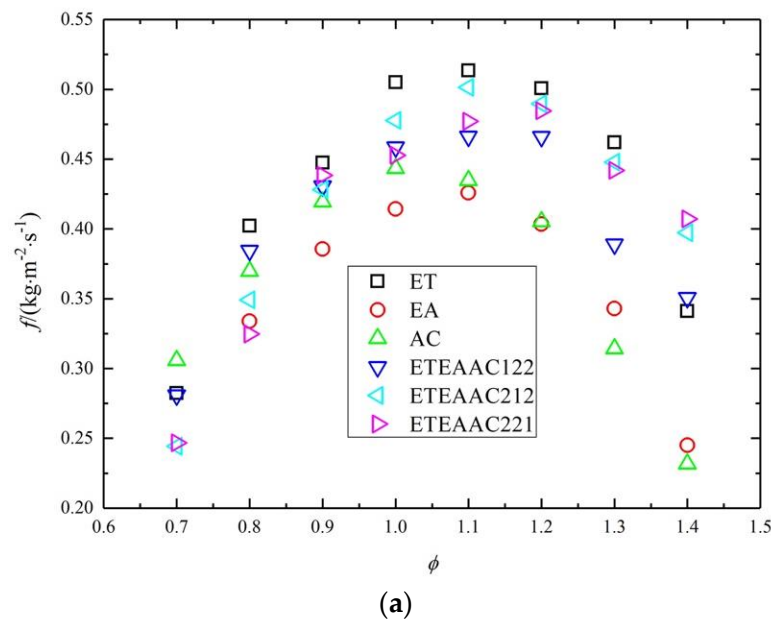


Figure 6. Cont.

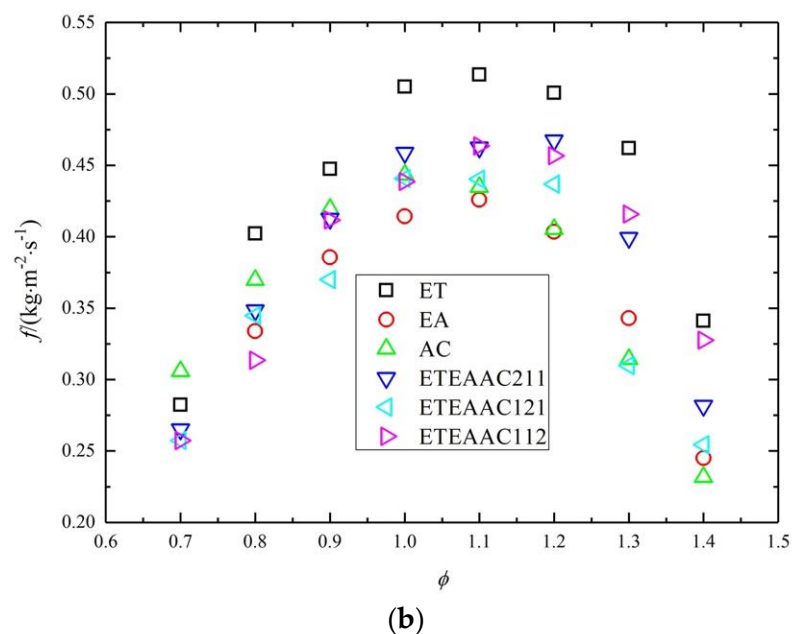


Figure 6. Laminar burning flux of the mixed fuels at $T_0 = 358$ K, $P_0 = 1$ bar, and $\phi = 0.7$ – 1.4 . (a) The laminar burning flux of ET/EA/AC/ETE AAC122/ETE AAC212/ETE AAC221, (b) The laminar burning flux of ET/EA/AC/ETE AAC211/ETE AAC121/ETE AAC112.

Figure 7 compares the laminar burning velocities of the simulation and the experimental results. The kinetic mechanism of small ester developed by Ahmed et al. [24] was used to calculate the laminar burning velocities. A skeletal mechanism was verified by comparing the calculation results of a detailed mechanism. The results of the skeletal mechanism and detailed mechanism are close. Simulation results overpredict the experimental laminar burning velocity. The relative deviation between the simulation and the experimental results of ETE AAC 112 is approximately 17.5%. The first reason for the difference between the simulation and the experimental results is that the radiation effect is not considered in the simulation model. Secondly, the model used in the Chemkin software is adiabatic, and there is no energy loss.

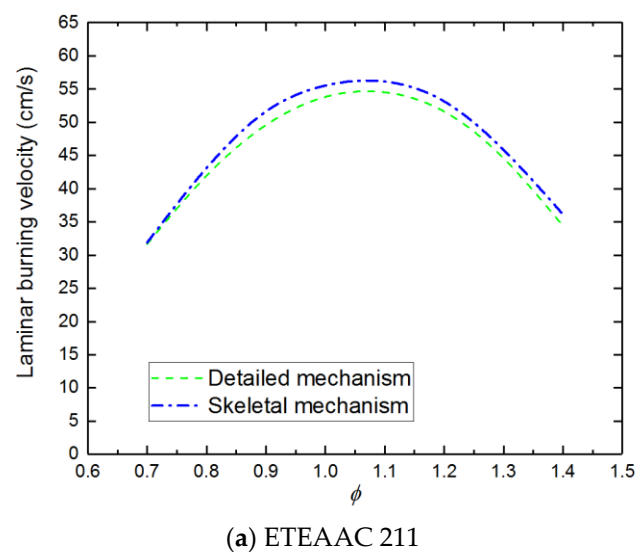
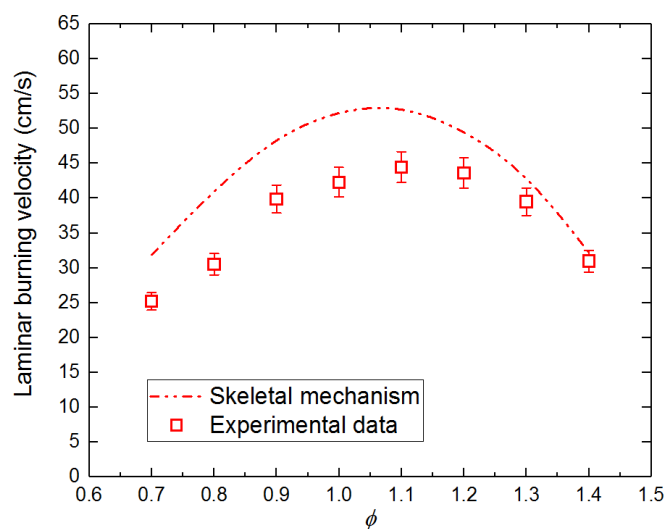


Figure 7. Cont.



(b) ETEAAC 112

Figure 7. Comparison of the laminar burning velocity of simulation and experimental results.

4.3. Mechanism Reduction

Based on the detailed mechanism [24], a directed relation graph with error propagation (DRGEP) was used to perform the mechanism reduction process. The detailed mechanism comprises 506 species and 2809 reactions, while the skeletal mechanism comprises 98 species and 642 reactions. Figure 8 presents the flame structure of ETEAAC 121 at $\phi = 1.0$. As the high-temperature product of the reaction, CO experiences a trend of increasing first and then decreasing. The reaction area is between 2.475 and 2.525 cm. The trails of the ethanol/acetone/ethyl acetate contents are similar, and the mole fraction of ethanol/acetone/ethyl acetate decreases rapidly in the reaction zone.

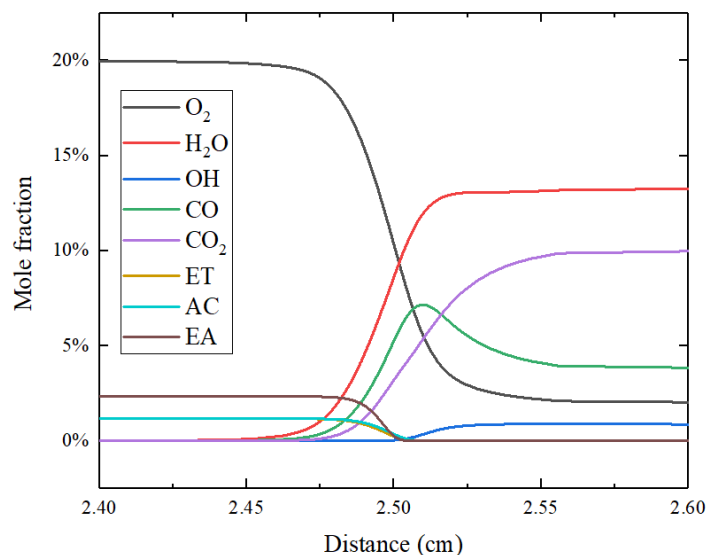
**Figure 8.** Flame structure of ETEAAC 121 determined with the skeletal mechanism at $\phi = 1.0$.

Figure 9 shows the sensitivity coefficient of EA consumption in ETEAAC 121 at $\phi = 0.7$, 1.0, and 1.3. One of the significant reactions at $\phi = 0.7$, 1.0, and 1.3 is $\text{O}_2 + \text{H} \rightleftharpoons \text{O} + \text{OH}$; it promotes EA consumption in rich mixtures, while it suppresses the combustion process of EA in lean mixtures. An H-abstraction reaction forming $\text{PC}_2\text{H}_4\text{OCOC}$ ($\text{EA} + \text{H} \rightleftharpoons \text{PC}_2\text{H}_4\text{OCOC} + \text{H}_2$) and the unimolecular decomposition of EA to form 2-acetic acid and ethane ($\text{EA} \rightleftharpoons \text{C}_2\text{H}_4 + \text{CH}_3\text{COOH}$) are important reactions for EA consumption.

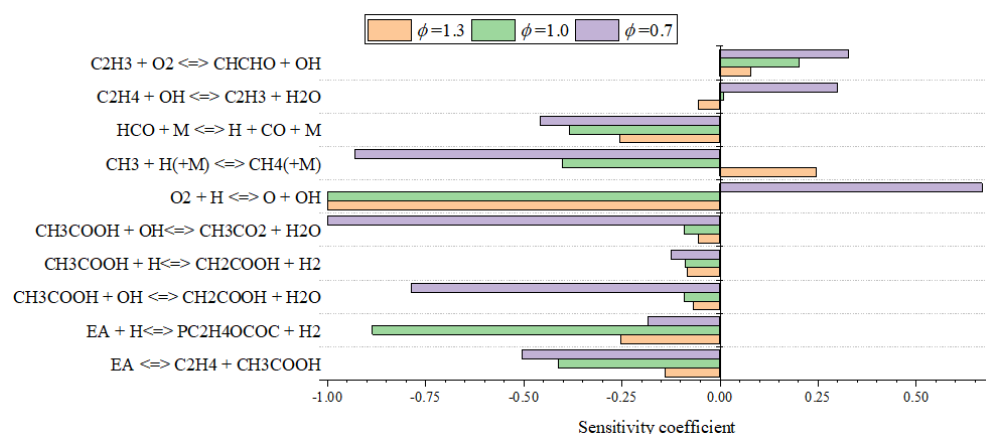


Figure 9. Sensitivity coefficient of EA consumption at $\phi = 0.7, 1.0,$ and 1.3 .

Figure 10 shows the main reaction paths of EA calculated with the skeletal and detailed mechanisms at $\phi = 1.1$. The skeletal mechanism preserves the key reaction path of EA, and there is not much difference in the flow rate of the skeletal and the detailed mechanisms. The maximum relative deviation of the flow rate is approximately 17% for the H-abstraction reaction forming SC2H4OCOC. It can be seen that the H-abstraction reactions forming SC2H4OCOC, PC2H4OCOC, and C2H5COCH are the most significant consumption pathways of EA combustion, accounting for 23.01%, 50.8%, and 8.41% in the detailed mechanism. The unimolecular decomposition to form acetic acid and ethane accounts for 17.77% and 17.06% of the detailed and the skeletal mechanisms, respectively. The rate of production of the main species and the reactions calculated by the skeletal mechanisms at $\phi = 1.1$ is shown in Table 2. The H-abstraction reaction $EA + H = PC_2H_4OCOC + H_2$ is the most important reaction of the EA consumption. Decomposition reactions are the main consumption path for PC2H4OCOC and SC2H4OCOC. In the reaction path calculated by the skeletal mechanism, PC2H4OCOC accounts for 50.8% of EA reaction consumption, while it is 23.01% for SC2H4OCOC, 17.77% for C2H4/CH3COOH, and 8.41% for C2H5OCOCH, respectively.

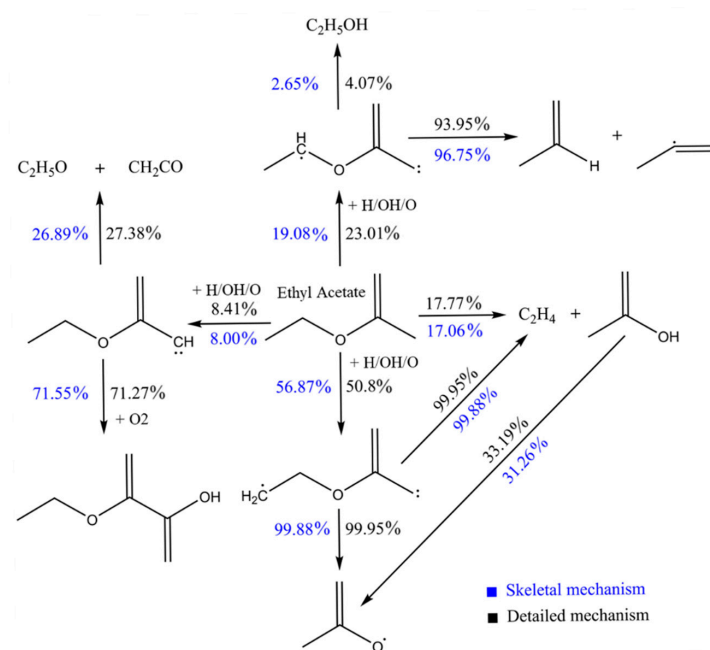


Figure 10. Comparison of the main reaction paths of EA calculated with the skeletal and the detailed mechanisms at $\phi = 1.1$.

Table 2. Rate of production for main species and reactions calculated by the skeletal mechanism at $\phi = 1.1$.

Species	Reaction	Rate of Production (Mole/cm ³ ·s)	Reaction Flux (%)
EA	EA + H = PC2H4OCOC + H2	-7.80×10^{-6}	44.39%
	EA = C2H4 + CH3COOH	-3.12×10^{-6}	17.77%
	EA + OH = SC2H4OCOC + H2O	-2.07×10^{-6}	11.79%
	EA + H = SC2H4OCOC + H2	-1.52×10^{-6}	8.68%
	EA + OH = PC2H4OCOC + H2O	-9.72×10^{-7}	5.53%
	EA + OH = C2H5OCOCH + H2O	-5.60×10^{-7}	3.19%
	EA + H = C2H5OCOCH + H2	-5.28×10^{-7}	3.00%
	EA + O = SC2H4OCOC + OH	-4.47×10^{-7}	2.54%
	EA + O = C2H5OCOCH + OH	-3.90×10^{-7}	2.22%
	EA + O = PC2H4OCOC + OH	-1.54×10^{-7}	0.88%
PC2H4OCOC	PC2H4OCOC = C2H4 + CH3CO2	-8.92×10^{-6}	99.95%
	PC2H4OCOC => C2H5OCOCH	-2.35×10^{-9}	0.03%
	H + VINACET = PC2H4OCOC	-1.62×10^{-9}	0.02%
SC2H4OCOC	SC2H4OCOC = CH3CHO + CH3CO	-3.81×10^{-6}	93.95%
	SC2H4OCOC => C2H5OCOCH	-1.65×10^{-7}	4.07%
	H + VINACET = SC2H4OCOC	-3.75×10^{-8}	0.93%
	SC2H4OCOC + O2 <=> VINCET + HO2	-3.42×10^{-8}	0.84%
	SC2H4OCOC + H = EA	-8.78×10^{-9}	0.22%

5. Conclusions

This study reported the laminar premixed characteristics including laminar burning velocity, Markstein length, Markstein number, and burning flux of ethanol/acetone/ethyl acetate mixed fuels at the initial temperature of 358 K, the initial pressure of 1 bar in a constant volume combustion chamber using equivalence ratios of 0.7 to 1.4. Based on the detailed chemical mechanism, a skeletal mechanism is obtained by DRGEP. The main conclusions of the study are as follows:

1. The order of the promoting effect of the concentrations of ET, AC, and EA on the laminar burning velocity is $ET > AC > EA$.
2. With the change of the equivalence ratio, the Markstein number presents a parabolic trend.
3. The maximum laminar burning flux appears at the equivalence ratio of 1.0–1.2, and the laminar burning flux of ETEAAC ternary fuel is closer to that of pure fuels on the lean side.
4. The experimental and the simulation results of laminar burning velocities have a good consistency, and the relative deviation of ETEAAC 112 is approximately 17.5%.
5. The reaction pathways show that H-abstraction reactions are significant for EA consumption; SC2H4OCOC and PC2H4OCOC are important species for EA combustion.

Author Contributions: Conceptualization, Y.L. and W.L.; methodology, H.L.; software, H.A.; validation, W.Z., Y.L. and C.X.; formal analysis, Y.L.; investigation, W.L.; resources, C.X.; writing—original draft preparation, Y.L.; writing—review and editing, W.L.; visualization, H.A.; funding acquisition, C.X. All authors have read and agreed to the published version of the manuscript.

Funding: This research was funded by the National Key R&D Program of China (2018YFB1501405), Basic Scientific Research Project of Zhejiang Technical Institute of Economics (JKY2021014), Ningbo major science and technology project (20212ZDYF020041), and Open Project of State Key Laboratory of Clean Energy Utilization, Zhejiang University (Grant No. ZJU-CEU2020001).

Institutional Review Board Statement: Not applicable.

Informed Consent Statement: Not applicable.

Acknowledgments: The authors are indebted to the National Key R&D Program of China (2018YFB1501405), Basic Scientific Research Project of Zhejiang Technical Institute of Economics (JKY2021014), Ningbo major science and technology project (20212ZDYF020041), and Open Project of State Key Laboratory of Clean Energy Utilization, Zhejiang University (Grant No. ZJU-CEU2020001) for funding this work.

Conflicts of Interest: The authors declare no conflict of interest.

References

1. Polverino, P.; Arsie, I.; Pianese, C. Optimal energy management for hybrid electric vehicles based on dynamic programming and receding horizon. *Energies* **2021**, *14*, 3502. [[CrossRef](#)]
2. Gao, J.; Jiang, D.; Huang, Z. Spray properties of alternative fuels: A comparative analysis of ethanol-gasoline blends and gasoline. *Fuel* **2007**, *86*, 1645–1650. [[CrossRef](#)]
3. Fernandez-Rodriguez, D.; Lapuerta, M.; German, L. Progress in the use of biobutanol blends in diesel engines. *Energies* **2021**, *14*, 3215. [[CrossRef](#)]
4. Kohse-Hoeninghaus, K.; Osswald, P.; Cool, T.A.; Kasper, T.; Hansen, N.; Qi, F.; Westbrook, C.K.; Westmoreland, P.R. Biofuel combustion chemistry: From ethanol to biodiesel. *Angew. Chem. Int. Edit.* **2010**, *49*, 3572–3597. [[CrossRef](#)]
5. Celik, M.B. Experimental determination of suitable ethanol-gasoline blend rate at high compression ratio for gasoline engine. *Appl. Therm. Eng.* **2008**, *28*, 396–404. [[CrossRef](#)]
6. Iodice, P.; Amoresano, A.; Langella, G. A review on the effects of ethanol/gasoline fuel blends on NO_x emissions in spark-ignition engines. *Biofuel Res. J. BRJ* **2021**, *8*, 1465–1480. [[CrossRef](#)]
7. Oxenham, L.; Wang, Y. A study of the impact of methanol, ethanol and the miller cycle on a gasoline engine. *Energies* **2021**, *14*, 4847. [[CrossRef](#)]
8. Iodice, P.; Cardone, M. Ethanol/Gasoline Blends as alternative fuel in last generation spark-ignition engines: A review on co and hc engine out emissions. *Energies* **2021**, *14*, 4034. [[CrossRef](#)]
9. Cooper, S.P.; Gregoire, C.M.; Mohr, D.J.; Mathieu, O.; Alturaifi, S.A.; Petersen, E.L. An experimental kinetics study of isopropanol pyrolysis and oxidation behind reflected shock waves. *Energies* **2021**, *14*, 6808. [[CrossRef](#)]
10. Zhao, Z.; Yu, X.; Huang, Y.; Shi, W.; Guo, Z.; Li, Z.; Du, Y.; Jin, Z.; Li, D.; Wang, T.; et al. Experimental study on combustion and emission of an SI engine with ethanol /gasoline combined injection and EGR. *J. Clean. Prod.* **2022**, *331*, 129903. [[CrossRef](#)]
11. Elfasakhany, A. Dual and ternary biofuel blends for desalination process: Emissions and heat recovered assessment. *Energies* **2021**, *14*, 61. [[CrossRef](#)]
12. Dhanarasu, M.; RameshKumar, K.A.; Maadeswaran, P. Effect of acetone as an oxygenated additive with used sunflower oil biodiesel on performance, combustion and emission in diesel engine. *Environ. Technol.* **2021**, 1–11. [[CrossRef](#)] [[PubMed](#)]
13. Dinesha, P.; Mohan, S.; Kumar, S. Experimental investigation of SI engine characteristics using Acetone-Butanol-Ethanol (ABE)—gasoline blends and optimization using particle swarm optimization. *Int. J. Hydrogen Energy* **2021**, *47*, 5692–5708. [[CrossRef](#)]
14. Sekularac, N.; Fang, X.H.; Shankar, V.; Baker, S.J.; Leach, F.C.P.; Davy, M.H. Development of a laminar burning velocity empirical correlation for combustion of iso-octane/ethanol blends in air. *Fuel* **2022**, *307*, 121880. [[CrossRef](#)]
15. Katoch, A.; Millan-Merino, A.; Kumar, S. Measurement of laminar burning velocity of ethanol-air mixtures at elevated temperatures. *Fuel* **2018**, *231*, 37–44. [[CrossRef](#)]
16. Aghsaee, M.; Nativel, D.; Bozkurt, M.; Fikri, M.; Chaumeix, N.; Schulz, C. Experimental study of the kinetics of ethanol pyrolysis and oxidation behind reflected shock waves and in laminar flames. *Proc. Combust. Inst.* **2015**, *35*, 393–400. [[CrossRef](#)]
17. Knorsch, T.; Zackel, A.; Mamaikin, D.; Zigan, L.; Wensing, M. Comparison of different gasoline alternative fuels in terms of laminar burning velocity at increased gas temperatures and exhaust gas recirculation rates. *Energy Fuel* **2014**, *28*, 1446–1452. [[CrossRef](#)]
18. Sileghem, L.; Alekseev, V.A.; Vancoillie, J.; Nilsson, E.J.K.; Verhelst, S.; Konnov, A.A. Laminar burning velocities of primary reference fuels and simple alcohols. *Fuel* **2014**, *115*, 32–40. [[CrossRef](#)]
19. Dirrenberger, P.; Glaude, P.A.; Bounaceur, R.; Le Gall, H.; Da Cruz, A.P.; Konnov, A.A.; Battin-Leclerc, F. Laminar burning velocity of gasolines with addition of ethanol. *Fuel* **2014**, *115*, 162–169. [[CrossRef](#)]
20. Zhang, S.; Lee, T.H.; Wu, H.; Pei, J.; Wu, W.; Liu, F.; Zhang, C. Experimental and kinetic studies on laminar flame characteristics of acetone-butanol-ethanol (ABE) and toluene reference fuel (TRF) blends at atmospheric pressure. *Fuel* **2018**, *232*, 755–768. [[CrossRef](#)]
21. Nilsson, E.J.K.; de Goey, L.P.H.; Konnov, A.A. Laminar burning velocities of acetone in air at room and elevated temperatures. *Fuel* **2013**, *105*, 496–502. [[CrossRef](#)]
22. Zhang, S.; Lee, T.H.; Wu, H.; Pei, J.; Wu, W.; Liu, F. Experimental and kinetical study of component volumetric effects on laminar flame speed of Acetone-Butanol-Ethanol (ABE). *Energy Fuel* **2018**, *32*, 6278–6292. [[CrossRef](#)]
23. Gong, J.; Zhang, S.; Cheng, Y.; Huang, Z.; Tang, C.; Zhang, J. A comparative study of n-propanol, propanal, acetone, and propane combustion in laminar flames. *Proc. Combust. Inst.* **2015**, *35*, 795–801. [[CrossRef](#)]

24. Ahmed, A.; Pitz, W.J.; Cavallotti, C.; Mehl, M.; Lokachari, N.; Nilsson, E.J.K.; Wang, J.; Konnov, A.A.; Wagnon, S.W.; Chen, B.; et al. Small ester combustion chemistry: Computational kinetics and experimental study of methyl acetate and ethyl acetate. *Proc. Combust. Inst.* **2019**, *37*, 419–428. [[CrossRef](#)]
25. Wang, Y.L.; Lee, D.J.; Westbrook, C.K.; Egolfopoulos, F.N.; Tsotsis, T.T. Oxidation of small alkyl esters in flames. *Combust. Flame* **2014**, *161*, 810–817. [[CrossRef](#)]
26. Osipova, K.N.; Dmitriev, A.M.; Shmakov, A.G.; Korobeinichev, O.P.; Minaev, S.S.; Knyazkov, D.A. Combustion of ethyl acetate: The experimental study of flame structure and validation of chemical kinetic mechanisms. *Mendeleev Commun.* **2019**, *29*, 690–692. [[CrossRef](#)]
27. Xu, C.; Zhou, K.; Li, X.; Zhong, A.; Oppong, F.; Wang, H.; Wu, S.; Zhou, W.; Wang, C. Laminar burning characteristics of two rice-husk-derived biofuels. *Energy Fuel* **2018**, *32*, 9872–9882. [[CrossRef](#)]
28. Xu, C.; Zhong, A.; Li, X.; Wang, C.; Sahu, A.; Xu, H.; Lattimore, T.; Zhou, K.; Huang, Y. Laminar burning characteristics of upgraded biomass pyrolysis fuel derived from rice husk at elevated pressures and temperatures. *Fuel* **2017**, *210*, 249–261. [[CrossRef](#)]
29. Xu, C.; Wang, H.; Oppong, F.; Li, X.; Zhou, K.; Zhou, W.; Wu, S.; Wang, C. Determination of laminar burning characteristics of a surrogate for a pyrolysis fuel using constant volume method. *Energy* **2020**, *190*, 116315. [[CrossRef](#)]
30. Xu, C.; Liu, W.; Zhang, B.; Liao, H.; He, W.; Wei, L. Experimental and numerical study on laminar premixed flame characteristics of 2-ethylfuran. *Combust. Flame* **2021**, *234*, 111631. [[CrossRef](#)]
31. Yang, Q.; Liu, Z.; Hou, X.; He, X.; Sjöberg, M.; Vuilleumier, D.; Liu, C.; Liu, F. Measurements of laminar flame speeds and flame instability analysis of E30-air premixed flames at elevated temperatures and pressures. *Fuel* **2020**, *259*, 116223. [[CrossRef](#)]
32. Kelley, A.P.; Law, C.K. Nonlinear effects in the extraction of laminar flame speeds from expanding spherical flames. *Combust. Flame* **2009**, *156*, 1844–1851. [[CrossRef](#)]
33. Luo, Z.; Oppong, F.; Wang, H.; Li, X.; Xu, C.; Wang, C. Investigating the laminar burning velocity of 2-methylfuran. *Fuel* **2018**, *234*, 1469–1480.
34. Liu, Y.; Liu, W.; Liao, H.; Zhou, W.; Xu, C. An experimental and kinetic modelling study on laminar premixed flame characteristics of ethanol/acetone mixtures. *Energies* **2021**, *14*, 6713. [[CrossRef](#)]